Trifluorocoumarino Cryptands as Photoprotonic Molecules: Basic Features and Theoretical Considerations

P. Buet, F. Kastenholz, and E. Grell*

Max-Planck-Institut für Biophysik, Kennedy-Allee 70, D-60596 Frankfurt, Germany

G. Käb, A. Häfner, and F. W. Schneider

Institut für Physikalische Chemie der Universität Würzburg, Am Hubland, D-97074 Würzburg, Germany

Received: March 26, 1999

The coupling between the fluorescence properties of the (trifluoromethyl)coumarino fluorophore and the protolytic state of the ion binding moiety of two fluorescent cryptands, **F221** and **F222**, is investigated experimentally by carrying out steady-state and time-resolved fluorescence measurements. The high-intensity fluorescence emission of the diprotonated state of the these alkali ion-selective indicators**,** characterized by quantum yields of 0.6 and 0.83 as well as by lifetimes of 5.3 and 5.6 ns, are markedly quenched upon deprotonation, which leads to the monoprotonated state with quantum yields of 0.07 and 0.02 as well as lifetimes of 1.0 and 0.19 ns, respectively. The corresponding pK_{a1} values are 7.07 for **F221** and 5.85 for **F222**. The formation of the fully deprotonated state of the fluorescent cryptands, characterized by pK_{a2} values of 10.6 and 9.3, respectively, is accompanied by a comparatively small additional reduction of the fluorescence quantum yield and lifetime. As a framework for the understanding of the pH-dependent fluorescence parameters, we suggest the concept of fluorescence quenching via photoinduced electron transfer (PeT), where the quenching process is assumed to be controlled by the pH-dependent availability of nonprotonated bridgehead N-atoms of the cryptand. These N-atoms act as electron donors with respect to the excited fluorophore, which functions as electron acceptor. In order to quantify the PeT energetics in the case of **F221** and its monoprotonated state, one-electron oxidation and reduction potentials are determined by cyclic voltammetry for the parent cryptand **[2.2.1]** and the fluorophore derivative **I** as suitable model compounds, respectively. Experimental redox data are supplemented by simple estimations of the electrostatic energy contributions for the intramolecular radical ion pair produced through photoinduced charge separation and by corrections for the hydration energies. The resulting thermodynamic driving forces for PeT in the deprotonated **F221** and its monoprotonated form show that PeT is favored for both of these species in water, where only a minor endergonic shift is observed for the monoprotonated as compared to the fully deprotonated compound. Therefore, the fully de- and the monoprotonated state of these fluorescent cryptands are regarded as being responsible for the reduction of the fluorescence quantum yield and the appearance of the second lifetime τ_2 at high pH. In contrast, PeT is expected to be completely blocked for the diprotonated state of these (trifluoromethyl)coumarino cryptands.

Introduction

The application of selective molecular recognitions for the development of functional chemical switching or information converting devices, based on interactions with electrons, ions, or photons, has been strongly stimulated by the progress achieved in supramolecular chemistry. In this context, chemical systems have been reported that interact selectively with a particular ion, for example with H^+ or an alkali ion, and where this interaction is linked to a photonic response.[1,2] Such features can be obtained by connecting an ion-selective ligand with a suitable fluorophore, as indicated schematically in Figure 1. Fluorescent compounds which show such properties are occasionally classified as fluorescent photoinduced electron transfer (PeT) sensors.[2]

Fluorescent cryptands exhibiting ion-selective binding properties represent typical examples of such chemical realizations.[3−9]

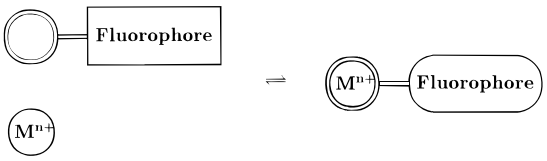

Figure 1. Schematic of a coordinating ligand connected to a suitable fluorophore within a supramolecular entity. The presence of a bound cation such as H^+ or M^{n+}, which alter the electronic and photophysical properties of the fluorophore either directly or indirectly via interaction with the ionophore, is mediated through a linker.

Although cryptand structures can be varied to be adapted to a chosen anion or metal ion,[1,10] the supporting or competing interaction of H^+ with their bridgehead nitrogens has to be considered too, provided properties around neutral pH are concerned. With regard to metal ion binding cryptands, not only the protonated state of the free ligand and the deprotonated state of its cryptate but also the state where H^+ and the metal ion

* To whom the correspondance should be adressed.

10.1021/jp9910690 CCC: $18.00
Published on Web 07/14/1999

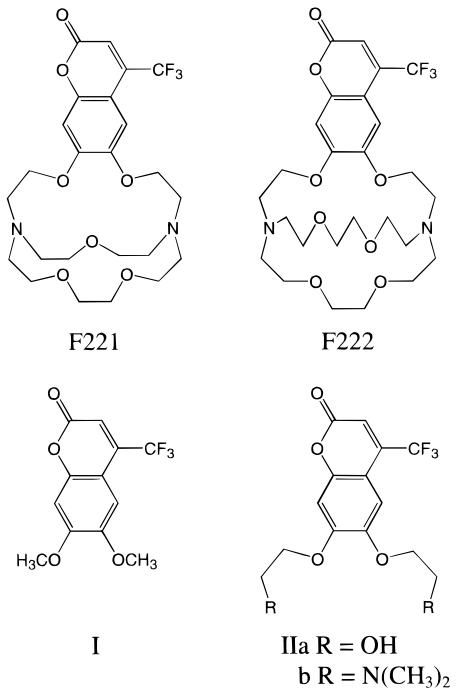

Figure 2. Chemical structures of (trifluoromethyl)coumarino cryptands and model compounds.

are bound, the protonated cryptate, need to be taken into consideration.

For a detailed understanding of the functional and spectral properties of such fluorescent cryptands, it's not only necessary to investigate and characterize their basic physicochemical properties but also to develop concepts to achieve a theoretical understanding of the mutual interaction between the metal ion coordinating unit and the linked fluorophore of the complete functional device.

In this article, we concentrate on the interaction of H^+ with a Na^+- and a K^+-selective (trifluoromethyl)coumarino cryptand, **F221** and **F222**,[6−9] which can be employed as fluorescent alkali ion indicators, as well as on the model compounds **I** and **II** (Figure 2). We report the relevant thermodynamic parameters of protolysis together with the steady-state and time-resolved fluorescence properties of the different protolytic states, which contribute to the understanding of the photoprotonic properties of these molecules.

In addition, we address the question regarding the mechanism by which the binding of protons to the cryptand moiety alters the fluorescence properties of the connected coumarin chromophore, i.e. the function of the fluorescent cryptands as selectively cation binding photoprotonic molecules. This shall be done in terms of simple considerations related to electron transfer theory. Therefore, the aim of this contribution consists of the combination of an experimental study and a theoretical analysis.

A first attempt to explain the pH dependence of **F221** and **F222** fluorescence quantum yield was based on the assumption that protonation leads to a more rigid nuclear framework of the cryptand, thereby restricting radiationless decay of the fluorescent singlet state of the coumarin moiety.[7,8] This concept was supported in a qualitative manner by semiempirical quantum chemical calculations for **F221** and its protonated states.[8,11] Moreover, the computations revealed that protonation leads to an increase of the electronic energy gap between the first excited singlet state S_1 and the next nearest triplet T_x of the coumarin chromophore. When discussed in the framework of the energy gap law, the increase of the S_1-T_x electronic energy gap induced by protonation was assumed to cause a reduction of the respective rate of intersystem crossing. Therefore, the efficiency of this $S_1 \rightarrow T_x$ intersystem crossing was believed to be responsible for the pH-dependent change of the fluorescence quantum yield, being high at low pH and decreasing with increasingly larger pH values.

However, the present working hypothesis assumes that photoinduced electron transfer from one of the two cryptand nitrogen atoms to the locally excited coumarin fluorophore is the operating mechanism of pH-dependent fluorescence quenching. This model is supported by the identification of the electronic nature of cryptand and fluorophore components of the fluorescent molecules. In our case, the cryptand moiety can be identified as electron donor, whereas the electron-poor coumarin chromophore acts as a potential electron acceptor, both of which are electronically coupled to each other via the nuclear framework of the cryptand.

The central electron transfer parameter addressed in the present work by means of cyclic voltammetry is the free energy of photoinduced electron transfer. In the present context, it is expected that the free energy $\Delta G°$ of electron transfer is the key parameter, which is controlled by the degree of protonation of the cryptand moiety and which provides the understanding of the pH dependence of **F221** and **F222** fluorescence.

Experimental Section

(a) Materials. *(1) Chemicals.* General chemicals were of analytical grade, supplied by Fluka or Merck. Special chemicals consist of 33% dimethylamine in absolute ethanol (quality grade purum, Fluka), acetonitrile (quality grade puriss., dried over molecular sieve, Fluka), (2-hydroxyethyl)trimethylammonium chloride (choline chloride, ChCl, quality grade microselect, Fluka), *N*-ethylmorpholine (quality grade microselect, Fluka), H_2SO_4 (quality grade Suprapur, Merck), 3,4-dimethoxyphenol (quality grade purum, Fluka), ethyl 4,4,4-trifluoroacetoacetate (quality grade purum, Fluka), and methanol (quality grade Uvasol, Merck). Dichloromethane was received from Merck in HPLC quality, distilled in an atmosphere of dry dinitrogen gas over P_2O_5 and filtered over basic Al_2O_3. Cellulose precoated thin layer chromatography (TLC) plates, thickness 0.1 mm, and silica gel 60 WF_{254}s precoated TLC sheets were purchased from Merck. Sephadex LH-20 was obtained from Pharmacia Fine Chemicals. 5,5-Diethylbarbituric acid (Veronal, Merck) was recrystallized from water, tetramethylammonium chloride ((TMA)Cl, Fluka), and tetramethylammonium hydroxide ((TMA)OH, Fluka) from ethanol−diethyl ether. The resistance of the MILLI-Q (Millipore) filtered water was higher than 17 MΩ/cm. All buffer solutions were prepared in LDPE (low-density polyethylene) flasks, and the pH adjustment was done without of a contact with a pH electrode to minimize trace contents of potassium.

(2) Cryptands. 4-(Trifluoromethyl)coumarino[6,7-*e*]-4,7,13,16,21-pentaoxa-1,10-diazabicyclo[8.8.5]tricosan (**F221**) and 4-trifluoromethylcoumarino[6,7-*e*]-4,7,13,16,21,24-hexaoxa-1,10-diazabicyclo[8.8.5]tricosan (**F222**) were synthesized and purified according to ref 7. Stock solutions of **F221** and **F222** were prepared in methanol Uvasol (ca. 5.0 mM) and kept at 5 °C. Calculations of concentrations were based on the extinction coefficients 10 500 M^{-1} cm^{-1}/351 nm and 11 400 M^{-1} cm^{-1}/356 nm, respectively. Aqueous solutions were obtained by adding the corresponding stock solution in methanol to the aqueous buffer solution so that the methanol content was not higher than 1% (v/v).

(3) Model Compounds. 6,7-Dimethoxy-4-(trifluoromethyl)-coumarin (**I**) was prepared from 3,4-dimethoxyphenol and ethyl 4,4,4-trifluoroacetoacetate according to the von Pechmann method, as described in ref 12, and crystallized from ethanol (60%): yellowish crytals; TLC, petroleum ether/ethyl acetate/methanol (50/30/20 (v/v/v)); R_f, 0.6; mp, 177−178 °C. ^{1}H NMR (300 MHz, $CDCl_3$): δ 6.94 (q, J = 0.8, 1H), 6.81 (s, 1H), 6.55 (q, J = 0.8, 1H), 3.90 (s, 3H), 3.85 (s, 3H). Anal. Calc for $C_{12}H_9O_4F_3$ (274.19): C, 52.57; H, 3.31. Found: C, 52.67; H, 3.42.

*6,7-Di(2′-hydroxyethoxy)-4-(trifluoromethyl)coumarin **(IIa)***. Compound **IIa** was synthesized according to ref 7. A 14 mg amount of the crude product was recrystallized from ethyl acetate. The solid residue was purified on a silica gel column using petroleum ether/ethyl acetate/methanol (50/30/20 (v/v/v)) as eluent. The fractions corresponding to a R_f value of 0.60 on silica gel TLC plates (same eluent) were collected and evaporated. The solid material was rechromatographed on Sephadex LH-20 using methanol. After evaporation and drying over P_2O_5, 10 mg of pure compound (70%) was obtained: mp, 81 °C. ^{1}H NMR (250 MHz, CD_3CO_2D): δ 7.20 (m, 1H), 7.07 (s, 1H), 6.76 (s, 1H), 4.18−4.29 (m, 4H), 4.00−4.09 (m, 4H). Anal. Calc for $C_{14}H_{13}F_3O_6$ (334.2): C, 50.3; H, 3.92. Found: C, 50.03; H, 4.15.

*6,7-Di(2′-(dimethylamino)ethoxy)-4-(trifluoromethyl)coumarin **(IIb)***. An 80 μL aliquot of 33% $NH(CH_3)_2$ in absolute ethanol was added slowly to 50 mg of 6,7-di(2′-iodoethoxy)-4-(trifluoromethyl)coumarin[7] in 6 mL of acetonitrile under nitrogen atmosphere and stirred for 30 h. The mixture was evaporated at 10 °C. The solid residue was dissolved in 50 mL of 0.01 M HCl and washed 3 times with 20 mL of diethyl ether. The pH of the resulting, combined aqueous phase was adjusted to 7.5 using 0.1 M NaOH solution. After extraction 3 times with 50 mL of CH_2Cl_2, the combined organic phase was evaporated. The resulting product was purified by preparative TLC employing cellulose plates by using the Partridge mixture (equilibrated upper phase of 1-butanol/water/acetic acid (40/50/10 (v/v/v)))[13] as eluent. Bands characterized by a single component and corresponding to a R_f value of 0.40 were scratched off, eluted with methanol, filtered, combined, and evaporated. The solid material was rechromatographed on Sephadex LH-20 using methanol. After evaporation and drying over P_2O_5, **IIb** was obtained as a yellowish oil (25 mg, 71%). ES-MS (methanol−acetonitrile): 389 $[M + H]^+$. The concentration determination of the stock solution in methanol Uvasol was based on the extinction coefficient of **IIa** in methanol (11 300 M^{-1} cm^{-1}/359 nm). Aqueous solutions prepared from the stock solution had a methanol content smaller than 1% (v/v).

(b) Spectra and Methods. *(1) Absorption Spectra.* Absorption spectra were recorded using an Uvikon 810 (Kontron), HP 8450A (Hewlett-Packard) diode array or an U-3000 (Hitachi) spectrophotometer coupled to a personal computer. All spectrophotometers were equipped with the double beam technology and thermostated cuvette holders and provided identical results.

(2) Fluorescence Spectra. Uncorrected emission and excitation spectra of the fluorescent compounds were obtained with a Spex Fluorolog 212 instrument, equipped with a 450 W xenon lamp as light source, interfaced to a personal computer and thermostated cuvette holders.

Corrected emission spectra were obtained on an Aminco Bowman series 2 luminescence spectrometer by multiplying uncorrected spectra with an emission correction factor. This factor was determined by using a calibrated light source.[14] The excitation wavelength was 360 nm; the emission spectra were recorded between 380 and 700 nm. Typical concentrations of the fluorescent compounds ranged between 5.0×10^{-6} and 5.0×10^{-5} M to provide similar fluorescence intensities for all samples (maximum difference, ±15%). The pH of the solutions before and after the measurement did not differ by more than 0.03. All experiments were carried out at 25 °C.

(3) Quantum Yield. The quantum yields of the fluorescent compounds were determined at different pH values, by employing the comparative method as described by Bridges in ref 15. As standard solution, a freshly prepared solution of 1.2×10^{-6} M quinine sulfate (qui) in 1 N H_2SO_4 was applied. For all samples including the standard solution, the absorption values (Abs_{sample} and Abs_{qui}, respectively) were measured at 360 nm using the Kontron spectrophotometer. Corrected fluorescence emission spectra of the samples and the standard were recorded between 380 and 700 nm and integrated in arbitrary units ($\int Fluo_{sample}$ and $\int Fluo_{qui}$, respectively). The quantum yields of the samples were then calculated using eq 1, where Φ_{qui} represents the quantum yield of the standard solution (0.57 at 360 nm), taken from ref 16. All the measurements were carried out at 25 °C.

$$\Phi_{sample} = \Phi_{qui} \frac{\int Fluo_{sample}}{\int Fluo_{qui}} \frac{Abs_{qui}}{Abs_{sample}} \quad (1)$$

(4) Time-Resolved Fluorescence. Fluorescence decays were recorded with a commercial nanosecond single-photon counting equipment (Edinburgh Instruments) using a thyratron controlled nanosecond flash lamp as excitation source. The obtained data were analyzed using an iterative deconvolution technique based on the Marquardt−Levenberg algorithm, as described elsewhere.[17,18] Excitation wavelength and pulse width were 358 nm and 1.5 ns, respectively.

The emission intensity decays were analyzed by employing a multiexponential decay model,

$$I(t) = \sum_i \alpha_i e^{-t/\tau_i} \quad (2)$$

where α_i are the preexponential factors related to the lifetimes τ_i.

In order to evaluate the time-resolved intensity decays of a pH-dependent equilibrium system which consists of two fluorescent states, it is necessary to derive a relation between the relative amplitudes obtained from the decay analysis and the relative concentrations of the involved states. Considering the protolytic reaction of a monoprotic acid characterized by the dissociation constant K_a (eq 3), the relative concentrations of LH^+ and L (%LH^+ and %L, respectively) are given by eq 4.

$$LH^+ \rightleftharpoons L + H^+ \qquad K_a = [L][H^+]/[LH^+] \quad (3)$$

$$\%LH^+ = 100\left(1 + \frac{K_a}{[H^+]}\right)^{-1} \quad \text{and}$$

$$\%L = 100\left(1 + \frac{[H^+]}{K_a}\right)^{-1} \quad (4)$$

The contribution of the relative amplitude A_L of the species L to the steady-state fluorescence emission can be obtained from eq 5, where %L represents the relative concentration of the species L in solution, and Φ_L and Φ_{LH^+} are the quantum yields of L and LH^+, respectively.

$$A_L = 100\frac{\%L\Phi_L}{\%L\Phi_L + (100 - \%L)\Phi_{LH^+}} \quad (5)$$

The rearrangement of eq 5 provides an expression of the relative concentration of L as a function of the relative amplitude A_L and the quantum yields of L and LH^+ according to eq 6. In

$$\%L = 100\left(1 + \frac{(100 - A_L)\Phi_L}{A_L\Phi_{LH^+}}\right)^{-1} \quad (6)$$

addition, the relative amplitude A_L of the species can also be obtained from decay studies as given in eq 7, where α_L (α_{LH^+}, accordingly) represents the preexponential factor associated with the lifetime τ_L (τ_{LH^+}, accordingly).

$$A_L = 100\frac{\alpha_L\tau_L}{\alpha_L\tau_L + \alpha_{LH^+}\tau_{LH^+}} \quad (7)$$

Therefore, the combination of eqs 4, 6, and 7 together with the data obtained from time-resolved fluorescence studies allows the determination of the K_a value.

(5) Spectrofluorimetric pH Titrations. Spectrofluorimetric titrations of **F221**, **F222**, and **IIb** were carried out using the Spex fluorimeter. The excitation wavelength was kept at 360 nm. The solution of the approximately 9×10^{-6} M fluorophore in 20 mM Veronal with or without 178.7 mM choline chloride, adjusted to a pH value around 8.5 with 100 mM (TMA)OH, was stirred in the 1 cm quartz cuvette with a magnetic bar and thermostated at 25 °C. The pH was reduced in a stepwise manner by adding small volumes of 10 mM, 100 mM, or 1 M HCl with Eppendorf micropipets. After every addition, the pH was measured by employing a specially designed combined microelectrode (Möller, Zurich) containing 500 mM (TMA)Cl in the reference compartment. Under these circumstances, KCl leakage as observed with standard microcalomel reference electrodes is omitted. Emission spectra were recorded between 380 m and 650 nm at typically 25 different pH values. After dilution correction, the intensities of a selection of 25 wavelengths was then analyzed using the nonlinear fitting program LETAGROP,[19−21] based on the least squares regression algorithm, to determine the dissociation constant according to the chosen model.

(6) Cyclic Voltammetry. Cyclic voltammetry (CV) data were obtained with the help and the equipment of M. Schmittel, A. Burghart, and H. Ammon at the Institute of Organic Chemistry of the University of Würzburg. As model compounds for the respective donor and acceptor components of the coumarino cryptand **F221**, the cryptand **[2.2.1]**, and the model compound **I** were used.

For CV measurements the respective substances were dissolved at ca. 10^{-3} M concentration in methylene chloride, which was used because alkylamino radicals, formed here through oxidation of [**2.2.1**], are known to decompose rapidly via deprotonation in solvents of not too low basicity (A. Burghart, personal communication). Tetrabutylammonium hexafluorophosphate was employed as supporting electrolyte of ca. 0.1 M concentration.

The CV equipment used consisted of a potentiostat model 362 obtained from Princeton Applied Research and an $x-y-t$ recorder PM 8271 from Phillips for current versus time plots. Working and second electrode platinum wires were used, while the electric potential of the working electrode was varied against a silver reference electrode. After preliminary potential sweeps were applied to locate the peak potentials, ferrocene was added as an internal standard (+0.39 V vs standard calomel electrode, where only minor changes are observed with different solvents). Scan rates were equal to 100 mV/s. All experiments were done at 25 °C.

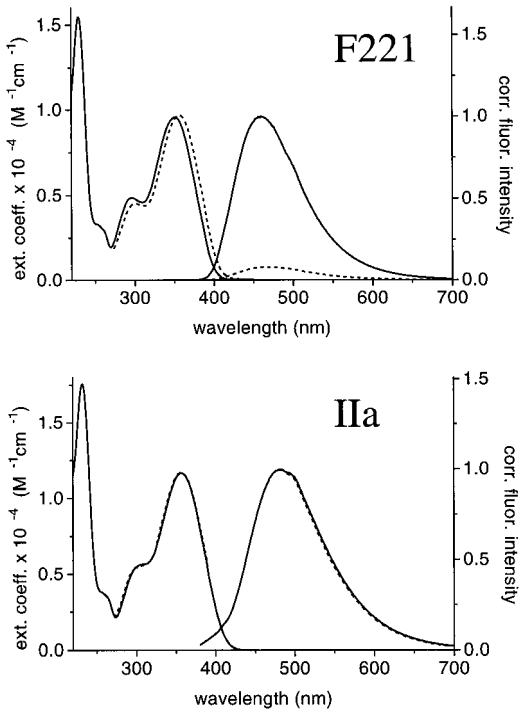

Figure 3. Absorption and normalized, corrected fluorescence emission spectra (λ_{ex} = 360 nm) of **F221** (5 μM) and **IIA** (5 μM) in 10 mM 3-aminopropionic acid/HCl, pH 3.50 (solid line), and in 10 mM Veronal/(TMA)OH, pH 8.50 (dashed line); 25 °C.

Results of Experimental Studies

(a) Steady-State Fluorescence. Due to its suitable spectral properties, the fluorescent coumarin residue has often been attached to ligands of biological interest for the purpose of sensitive and convenient analytical determinations. In order to achieve the maximum absorption and fluorescence emission at comparatively long wavelengths, we have introduced the trifluoromethyl group in position 4 of the coumarin residue (Figure 2). In Figure 3, the representative absorption and corrected fluorescence emission spectra of **F221** in its diprotonated form and **IIa** at pH 3.5 are shown. Under these conditions, the absorption maxima are in the range of 355 nm (lower for **F221** than for **IIa**), characterized by extinction coefficients of about 1.1×10^4 M^{-1} cm^{-1} (cf. Table 1). The fluorescence emission of this protolytic state exhibits a maximum intensity at 460 nm for **F221** and at 482 nm for **IIa** (Table 1) and a comparatively high quantum yield (cf. Table 2). The same general characterizations are valid for the cryptand **F222** and for the other two model compounds, **I** and **IIb**, under the same experimental conditions. Details of the spectral parameters are given in Tables 1 and 2.

As the consequence of a pH increase, for example up to pH 8.5, the fluorescence emission intensities of **I** and **IIa** remain nearly unchanged, whereas those of the model compound **IIb**, **F221**, and **F222** are markedly decreased, which is attributed to the predominant formation of the monoprotonated state FH^+ (Figure 4). The quantum yields at pH 8.5 are nearly 10 times lower than those of the diprotonated states (Table 2). A further increase of the pH is expected to lead to the formation of the fully deprotonated state (F in Figure 4). However, above pH

TABLE 1: Spectral Parameters of Absorption (Extinction Coefficient ϵ and λ_{max}) and Fluorescence[a] (Emission λ_{max}) of Fluorescent Cryptands and Model Compounds at pH 3.50 and 8.50; 25 °C

compd	pH (buffer[b])	ϵ (M^{-1} cm^{-1})/ λ_{max}[c] (nm)			λ_{max}^{em}[c] (nm)
F221	pH 3.5 (A)	15 460/229	4 900/296	9 600/351	460
	pH 8.5 (V)	*d*	4 500/300	9 700/356	468
F222	pH 3.5 (A)	17 900/231	5 800/297	11 700/354	468
	pH 8.5 (V)	*d*	5 200/303	11 900/359	473
I	pH 3.5 (A)	14 800/231	4 200/301	9 300/360	482
	pH 8.5 (V)	*d*	4 200/299	9 300/360	483
IIa	pH 3.5 (A)	17 530/231	5 500/301	11 600/357	482
	pH 8.5 (V)	*d*	5 500/300	11 700/356	482
IIb	pH 3.5 (A)	*d*	6 400/296	10 700/350	468
	pH 8.5 (V)	*d*	5 800/302	10 900/357	477

[a] Determined from corrected emission spectra; excitation always at 360 nm. [b] (A), 10 mM 2-aminopropionic acid/HCl; (V), 10 mM Veronal/(TMA)OH. [c] Accuracy ±3 nm. [d] Not determined.

TABLE 2: Quantum Yields of Fluorescent Cryptands and Model Compounds at Different pH Values; 25 °C

	quantum yield[a]				
compd	pH 3.5 (A)[b]	pH 7.5 (V)[c]	pH 7.5 (N)[d]	pH 7.5 (V, ChCl)[e]	pH 8.5 (V)[c]
F221	0.60	0.16	0.18	0.26	0.09
F222	0.83	0.019	0.018	0.022	0.016
I	0.32	*f*	*f*	*f*	0.35
IIa	0.33	0.35	*f*	0.35	0.33
IIb	0.48	0.14	*f*	0.18	0.06

[a] Estimated error: 10%. [b] (A), 10 mM 2-aminopropionic acid/HCl. [c] (V), 10 mM Veronal/(TMA)OH. [d] (N), 5 mM *N*-ethylmorpholine/HCl. [e] (V, ChCl), (V) containing 182.3 mM ChCl. [f] Not determined.

$$FH_2^{2+} \underset{}{\overset{K_{a1}}{\rightleftharpoons}} FH^+ + H^+ \overset{K_{a2}}{\rightleftharpoons} F + 2H^+$$

Figure 4. Reaction system of protolysis of cryptands **F221**, **F222**, and **IIb**, characterized by two macroscopic dissociation constants K_{a1} and K_{a2}. The monoprotonated state FH^+ consists in reality of two microscopic states.

8.8 the lactone form of the (trifluoromethyl)coumarino residue is not stable in aqueous solution. Hydrolysis leads under such conditions to ring opening, which affects the absorption spectrum (intensity decrease of the 295 nm and 355 nm bands) and causes a loss of fluorescence properties.

In order to determine the acidity constants (pK_a values) of **F221**, **F222**, and **IIb**, spectrofluorometric pH titrations are carried out by applying a suitable electrode system in order to avoid partial K^+ complexation by these ligands due to KCl diffusion out of the reference electrode. Such experiments have been carried out at low ionic strength in 20 mM Veronal buffer as well as in the additional presence of 178.7 mM choline chloride at a mean ionic strength of about 186 mM. In Figures 5 and 6, two representative spectrofluorometric pH titrations between pH 8.46 and 3.95 for **F221** and between 8.64 and 5.60 for **IIb** are shown. Except for the slightly more intense emission shoulder of **F221** at about 430 nm, the spectra as well as the spectral changes of cryptand and model compound are similar, although the changes are observed at different pH values. The evaluation of the emission intensities at 25 different wavelengths at the chosen pH values is done by employing the program LETAGROP after carrying out the volume corrections of the measured intensities.[19−21] Above pH 8.5, a small bathochromic shift of the fluorescence emission is observed, which is attributed to a contribution of the fully deprotonated state.

Because the titrations shown in Figure 5 and 6 cover essentially only the first deprotonation step, i.e. the transition from FH_2^{2+} to FH^+, the evaluation was initially based on a model corresponding to a monoprotic acid leading to a single

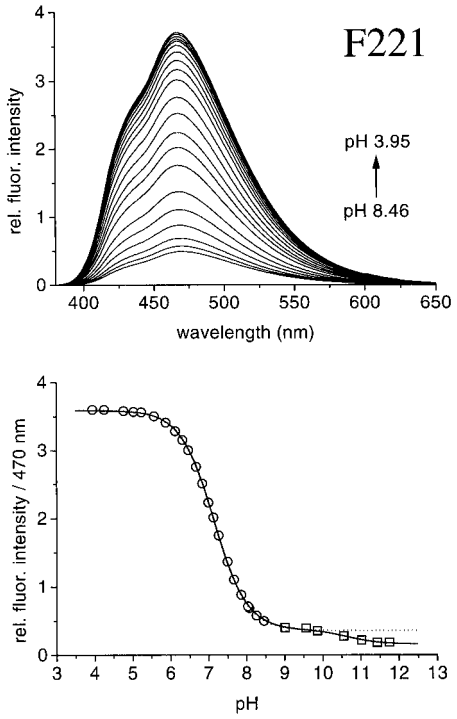

Figure 5. (Top) Spectrofluorimetric (λ_{ex} = 360 nm) pH titration of 20.7 μM **F221** with 0.01, 0.1, and 1 M HCl, starting in 20 mM Veronal/(TMA)OH containing 178.7 mM ChCl, pH 8.46; 25 °C. The emission spectra are dilution corrected. (Bottom) Semilogarithmic plot of the emission intensity at 470 nm versus pH (○, from spectrofluorimetric titration; □, from kinetics of hydrolysis). The solid line corresponds to a theoretical curve for the deprotonation of a diprotic acid with pK_{a1} and pK_{a2} values of 7.15 and 10.6. The dashed line represents the fluorescence level of the monoprotonated state.

pK_a value, denoted pK_a^{SF}. The corresponding values are given in Table 3 for high and low ionic strength. Having determined the pK_a^{SF} values of both fluorescent cryptands, the quantum yields of the state FH^+ can now also be estimated from the data observed at different pH values. For FH^+ a quantum yield around 0.07 results for **F221** and about 0.02 for **F222**.

Since the second deprotonation step cannot be investigated by direct titration above pH 8.8 (hydrolysis of the lactone bond), a different procedure has to be applied for the determination of the second pK_a, which is only applied under low ionic strength conditions. Different concentrations of (TMA)OH in 20 mM ethanolamine/HCl are added to solutions of the fluorescent cryptands in 20 mM ethanolamine/HCl, originally adjusted to pH 8.12, under vigorous stirring within about 1 s, and the rate of hydrolysis at the new, constant pH value (pH 9.0 and higher) is recorded spectrofluorimetrically. The resulting dependences

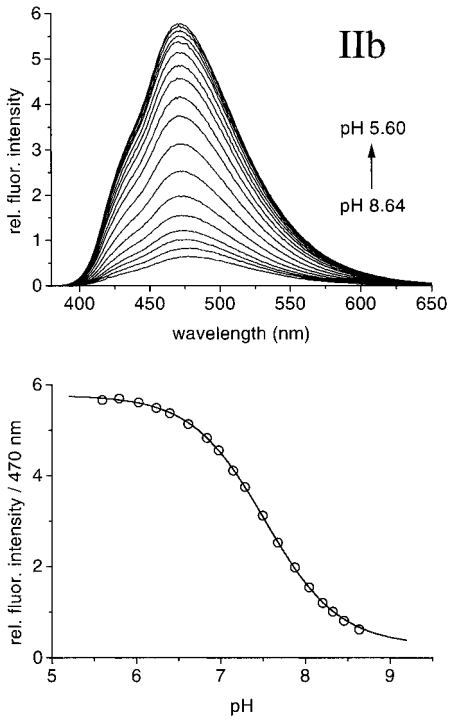

Figure 6. (Top) Spectrofluorimetric (λ_{ex} = 360 nm) pH titration of 20.1 μM **IIb** with 0.01, 0.1, and 1 M HCl, starting in 20 mM Veronal/(TMA)OH containing 178.7 mM ChCl, pH 8.64; 25 °C. The emission spectra are dilution corrected. (Bottom) Semilogarithmic plot of the emission intensity at 470 nm versus pH. The solid line corresponds to a theoretical curve for the deprotonation of a monoprotic acid according to eq 4 with a pK_a^{SF} value of 7.52.

TABLE 3: Dissociation Constants of Protolysis of Fluorescent Cryptands and Model Compounds in the Absence and Presence of an Electrolyte As Determined by Spectrofluorimetric Titration and from Fluorescence Lifetime Amplitudes; 25 °C

		monoprotic acid model		diprotic acid model	
compd	buffer[a]	pK_a^{SF} [b]	pK_a^{FL} [c]	pK_{a1} [b]	pK_{a2} [d]
F221	(V)	7.01 ± 0.03	*e*	7.07 ± 0.03	10.6 ± 0.7[f]
	(V, ChCl)	7.13 ± 0.03	*e*	*e*	*e*
F221	(V)	5.85 ± 0.03	*e*	5.85 ± 0.03	9.3 ± 0.3[f]
	(V, TMACl)	5.95 ± 0.03	6.2 ± 0.1[g]	*e*	*e*
IIb	(V)	7.45 ± 0.03	*e*	*e*	*e*
	(V, ChCl)	7.52 ± 0.03	*e*	*e*	*e*

[a] (V), 20 mM Veronal/(TMA)OH; (V, ChCl), (V) containing 178.7 mM ChCl; (V, (TMA)Cl), (V) containing 178.7 mM (TMA)Cl. [b] Determined by spectrofluorimetric titration. [c] Determined from fluorescence lifetime amplitudes. [d] Determined from kinetic studies of hydrolysis. [e] Not determined. [f] 20 mM ethanolamine/HCl. [g] 178.7 mM ChCl instead of (TMA)Cl.

can be fitted with a single exponential and allows the determination of the back-extrapolated value of the amplitude at time zero, which corresponds to the fluorescence intensity at the desired pH of the corresponding hydrolysis experiment. The reciprocal decay times determined in this manner at different, high-pH values are linearly dependent on [OH^-]; the resulting hydrolysis rate constants are 11.9 M^{-1} s^{-1} for **F221** and 8.8 M^{-1} s^{-1} for **F222** at 25 °C. The high-pH part of Figure 5 shows the fluorescence intensities of **F221** at 470 nm, extrapolated from the results of the kinetic **F221** hydrolysis study, as described before. The evaluation of the combined set of data employing LETAGROP, now based on a model for a diprotic acid, provide both macroscopic pK_a values, pK_{a1}, and pK_{a2}. These pH-dependent fluorescence properties provide singlet excited pK_a values; the corresponding values for **F221** and **F222** are given in Table 3. The indicated pK_a^{SF} values, related to the initial analysis due to a monoprotic acid, correspond to the pK_{a1} values of the expanded model (diprotic acid). In addition, it is estimated from this study that the quantum yield of the state F (cf. Figure 4) is <0.04 for **F221** and <0.009 for **F222**.

Although the pK_a values are slightly higher in the presence of choline chloride, the effect of the ionic strength appears to be comparatively small. Our results indicate that the pK_{a1} value depends on the structure of the compound in a rather sensitive manner. Whereas the value of **F221** is only about 0.4 units lower than that of the model compound **IIb**, the corresponding value for **F222**, however, is as much as 1.6 units lower (Table 3). This is a surprising result, because the pK_{a1} value of the parent cryptand **[2.2.2]**[22] is similar to that of the model compound **IIb** and is only about 0.3 units lower than that of **[2.2.1]**.[22] This may indicate that the structure of FH_2^{2+} or FH^+ of **F222** differs from the corresponding one of **F221**. Such a structural difference could be due to different fractions of H^+ located within the cavity of the cryptands, as suggested earlier for **[2.2.2]**.[23] Because pK_{a2} values of **F221** and **F222** are similar to those reported for **[2.2.1]** and **[2.2.2]**,[22] it appears likely that the structural difference can be assigned to the state FH_2^{2+}.

(b) Time-Resolved Fluorescence. Because of the large fluorescence emission intensity differences between the states FH_2^{2+} and FH^+, one has to assume that the corresponding fluorescence lifetimes differ, too. The fluorescence decays of **F221**, **F222**, and **IIb** at pH 3.5 as well as of the model compounds **I** and **IIa** between pH 3.5 and pH 8.5 are characterized by a single lifetime (τ_1) ranging between 4.1 and 5.6 ns (cf. Figure 7a,c; Table 4). At higher pH values, the decay curves of **F221, F222**, and **IIb** can no longer be evaluated on the basis of a single exponential. In order to achieve satisfactory fits, an additional, shorter decay time (τ_2) around 1 ns or lower has to be included, as observed earlier.[24] As an illustrative example, Figure 7b shows the fluorescence decay of **F222** at pH 7.5. The result clearly shows that no reasonable fit can be achieved on the basis of a single lifetime. However, the lifetime of **I** and **IIa** also remains at high pH. Time constants and the corresponding amplitudes are summarized in Table 4. As a general trend, one can conclude that in the cases of **F221**, **F222**, and **IIb** the amplitude A_1 (associated with τ_1) decreases with increasing pH, whereas the amplitude A_2 (corresponding to τ_2) increases. Therefore, we assign A_2 and τ_2 to the protolytic state FH^+ and, thus, A_1 and τ_1 to FH_2^{2+}. As indicated by the results obtained at pH 7.5 in the absence and presence of 182.3 mM choline chloride, the difference in ionic strength does not significantly change the values of the decay parameters.

In order to check the assignment mentioned before, the fluorescence decay of **F222** has been studied at five different pH values in the presence of 180 mM choline chloride to achieve an approximate mean ionic strength of 200 mM. The values of both lifetimes as well as of the corresponding amplitudes obtained at the different pH values are given in Table 5. Also here, two different life times had to be considered. In order to obtain directly comparable values for the pH dependence of both amplitudes, the decay data observed at all five pH values were fitted with an identical set of mean lifetimes (τ_1 = 5.4 ns and τ_2 = 0.19 ns). The corresponding amplitudes A'_1 and A'_2 are also given in Table 5. In Figure 8, a plot of the relative concentrations, obtained from the relative amplitudes according to eq 6, versus pH is shown. Fitting this data, according to eq 4, on the basis of a monoprotic dissociation equilibrium (according to eq 3) between the states L (corresponding to FH^+)

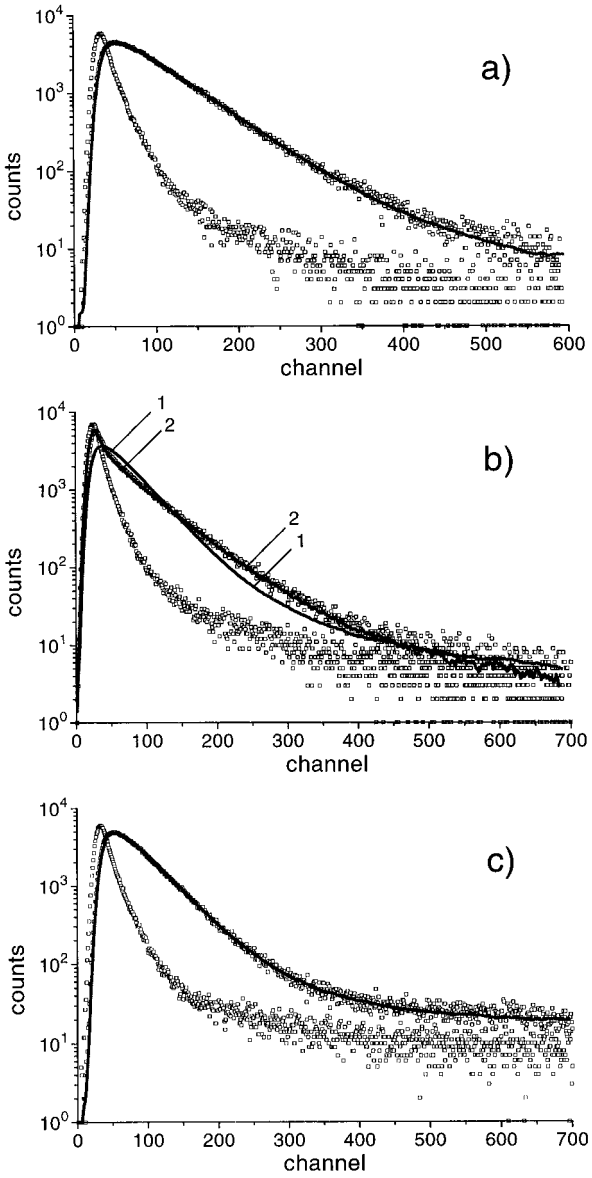

Figure 7. Fluorescence decay experiments showing the time-resolved 1.5 ns lamp pulse and the combined signal consisting of lamp pulse and fluorescence decay (time calibration, 0.101 ns/channel) of (a) 64.8 μM **F222** in 10 mM β-alanine/HCl, pH 3.5 (solid line corresponds to a single τ value of 5.59 ns), (b) 63.9 μM **F222** in 10 mM Veronal/(TMA)OH, pH 7.5 (line 1 corresponds to a single τ value of 4.29 ns, line 2, to a biexponential decay with $\tau_1 = 5.37$ ns and $\tau_2 = 0.19$ ns), and (c) 46.8 μM **IIa** in 10 mM Veronal/(TMA)OH, pH 7.5 (solid line corresponds to a single τ value of 4.20 ns). Amplitudes are given in Table 4. Excitation at 358 nm, emission at 470 nm; 25 °C.

and LH^+ (corresponding to FH_2^{2+}) leads to a pK_a^{FL} of 6.2, which is consistent with data obtained from spectrofluorimetric titrations (cf. Table 3). This result also confirms the assignement of τ_1 and τ_2, as mentioned before. Because each protolytic state is characterized by a single nanosecond decay time, our results provide no evidence for the existence of different ligand conformers in a single protolytic state, as discussed earlier.[25] Furthemore, the lifetime of the state FH^+ of **F221** is estimated to be 1.0 ns.

(c) Cyclic Voltammetry. In order to estimate, by using the Weller equation (see eq 11), the energetics of photoinduced electron transfer which is assumed to cause quenching of the locally excited state of deprotonated trifluorocoumarino cryptands, the one-electron oxidation and one-electron reduction potentials of the electron donor (amino groups of cryptand moiety) and the electron acceptor (coumarin chromophore), respectively, has to be determined.

Due to weak electronic coupling between the assumed donor groups and the acceptor chromophore (no charge transfer band could be observed in absorption spectra), the cryptand **[2.2.1]** and the coumarin fluorophore **I** are used as model compounds for **F221** as mentioned above. CV data for **F222** or model compounds thereof were not measured, because they are assumed not to differ significantly from the properties of **F221**.

TABLE 4: Time-Resolved Fluorescence of Fluorescent Cryptands and Model Compounds at Different pH Values[a]

		lifetime		% rel. amplitude		
compd	pH (buffer[b])	τ_1[c] (ns)	τ_2[c] (ns)	A_1	A_2	χ^2 [d]
F221	pH 3.5 (A)	5.30 ± 0.01		100		1.16
	pH 7.5 (V)	4.72 ± 0.01		100		3.23
		5.3 ± 0.3	1.22 ± 0.06	84	16	1.24
	pH 7.5	4.74 ± 0.01		100		1.58
	(V, ChCl)	5.0 ± 0.3	1.1 ± 0.1	91	9	1.13
	pH 8.5 (V)	2.72 ± 0.01		100		7.04
		4.60 ± 0.05	0.96 ± 0.02	50	50	1.14
F222	pH 3.5 (A)	5.59 ± 0.01		100		1.35
	pH 7.5	4.29 ± 0.01		100		27.1
	(V, ChCl)	5.37 ± 0.02	0.19 ± 0.02	69	31	1.32
I	pH 3.5 (A)	4.13 ± 0.01		100		1.23
	pH 8.5 (V)	4.14 ± 0.01		100		1.21
IIa	pH 3.5 (A)	4.21 ± 0.01		100		1.02
	pH 7.5 (V)	4.20 ± 0.01		100		1.10
	pH 8.5 (V)	4.16 ± 0.01		100		1.05
IIb	pH 3.5 (A)	5.38 ± 0.01		100		1.06
	pH 7.5 (V)	5.02 ± 0.01		100		1.76
		5.21 ± 0.01	0.41 ± 0.06	92	8	1.12
	pH 7.5	5.09 ± 0.01		100		1.84
	(V, ChCl)	4.61 ± 0.05	11.4 ± 0.8	90	10	1.19
	pH 8.5 (V)	3.66 ± 0.01		100		7.66
		4.71 ± 0.02	0.43 ± 0.02	68	32	1.10

[a] Relative amplitudes (A_i) are obtained from lifetimes (τ_i) and preexponential factors (α_i) as given in eq 7. Analysis is related to a mono- or biexponential fluorescence decay; 25 °C. [b] (A), 10 mM 2-aminopropionic acid/HCl; (V), 10 mM Veronal/(TMA)OH; (V, ChCl), (V) containing 182.3 mM ChCl. [c] Standard deviations related to the internal consistency of the achieved fit. [d] Reduced weighted sum of squares of deviations.

TABLE 5: Time-Resolved Fluorescence of F222 in 20 mM Veronal/(TMA)OH Containing 180 mM ChCl at Different pH Values; 25 °C[a]

	lifetime		% rel amplitude				
pH	τ_1[b] (ns)	τ_2[b] (ns)	A_1	A_2	A'_1	A'_2	χ^2 [c]
6.44	5.34 ± 0.01		100				1.32
	5.40 ± 0.01	0.54 ± 0.01	97.4	2.6	97.0	3.0	1.19
6.94	5.16 ± 0.01		100				6.1
	5.43 ± 0.01	0.26 ± 0.02	89.6	10.4	89.6	10.4	1.46
7.48	4.43 ± 0.01		100				27
	5.41 ± 0.02	0.19 ± 0.01	71.6	28.4	71.7	28.3	1.71
7.97	2.48 ± 0.01		100				49
	5.20 ± 0.03	0.12 ± 0.01	46.8	53.2	45.6	54.4	1.52
8.48	0.77 ± 0.01		100				20
	4.83 ± 0.07	0.17 ± 0.02	26.3	73.7	25.0	75.0	1.40

[a] Lifetimes (τ_i) and relative amplitudes (A_i) evaluated according to a mono- and biexponential fluorescence decay. The amplitudes A'_i refer to the evaluation of a biexponential decay with fixed values of $\tau_1 = 5.4$ ns and $\tau_2 = 0.19$ ns for all pH values. [b] Standard deviations related to the internal consistency of the achieved fit. [c] Reduced weighted sum of squares of deviations related to the fits based on τ_1, τ_2, A_1, and A_2 given in the table. The χ^2 values obtained from the fits related to the single set of fixed τ_1 and τ_2 values for the determination of A'_1 and A'_2 did not differ more than 8% from the previous ones and are not listed.

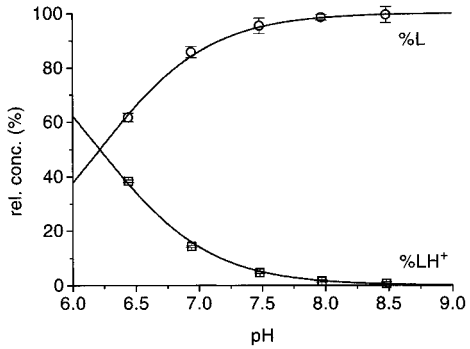

Figure 8. pH dependence of time-resolved fluorescence of **F222**: Plot of the relative concentrations of protolytic states L and LH^+, where L and LH^+ correspond to the states FH^+ and FH_2^{2+} in Figure 4, as calculated from the amplitudes A'_1 and A'_2 (cf. Table 5) according to eq 6. The solid line corresponds to a theoretical curve with a pK_a^{FL} value of 6.2 related to the dissociation of a monoprotic acid.

TABLE 6: Peak Potentials, E_p, and Potentials at Half Peak Height of Current, $E(I_p/2)$, for the One-Electron Oxidation of [2.2.1] and the One-Electron Reduction of Coumarin Chromophore I in Methylene Chloride As Determined by CV with Respect to the Equilibrium Redox Potential of the Standard Calomel Electrode; $T = 25$ °C

	E_p^{ox} [a] (Volt)	E_p^{red} [b] (Volt)	$(E_p^{ox} + E_p^{red})/2$ (Volt)	$E(I_p^{ox}/2)^a$ (Volt)	$E(I_p^{red}/2)^b$ (Volt)
[2.2.1]	+1.23	+1.07	+1.15	+1.13	
I		−1.66			−1.56

[a] Superscript ox indicates electric potential or current during anodic potential sweep. [b] Superscript red indicates electric potential or current during cathodic potential sweep.

Table 6 shows the anodic and cathodic peak potentials E_p^{ox} and E_p^{red}, respectively, the mean value calculated therefrom and the anodic and cathodic potentials at half peak height, $E(I_p^{ox}/2)$ and $E(I_p^{red}/2)$, for the one-electron oxidation of **[2.2.1]** and the one-electron reduction of **I** in CH_2Cl_2.

Both redox reactions are observed to be almost irreversible, although the oxidation of [**2.2.1]** exhibited an unexpected, remarkable degree of reversibility, while the radical anion of the coumarin chromophore turned out to be so unstable that no current peak could be observed during the anodic sweep. Since the mean value of E_p^{ox} and E_p^{red} for **[2.2.1]** is found to nearly coincide with $E(I_p^{ox}/2)$, we take the electric potential values at half of the current peak, $E(I_p^{ox}/2)$ and $E(I_p^{red}/2)$, respectively, as the most accurate measures of the true one-electron equilibrium redox potentials. Hence, we obtain a free energy of reaction $\Delta G° = +1.13$ eV $- (-1.56$ eV$) = +2.69$ eV for the one-electron reduction of **I** by [**2.2.1]** in the electronic ground state of redox reactants at infinite distance in methylene chloride.

Theoretical Considerations

The electronic structure of the coumarino cryptands **F221** and **F222** is that of a weakly coupled donor−acceptor system and reveals that these cation-sensitive fluorescent compounds belong to a general class of fluorescent PeT sensors, which respond to the presence of cationic species (metal ions, protons) by selective binding and a change in the efficiency of an intramolecular fluorescence quenching via photoinduced electron transfer.[26] To rationalize the pH-dependent function of these supramolecular photoprotonic molecules, the following basic elements of electron transfer (eT) theory are applied.

(a) Elements of Electron-Transfer Theory. For a weakly coupled electronic donor−acceptor system in solution, electron transfer from the donor to the acceptor may be described by Fermi's golden rule,

$$w_{i\to f} = \frac{2\pi}{\hbar}|V_{if}|^2\rho(E_f) \tag{8}$$

which, in the present case, states that the rate of electronic transition $w_{i\to f}$ is proportional to the square of the electronic interaction matrix element $V_{if} = V_{DA}$ and to the density of final states $\rho(E_f)$ evaluated for the equilibrated initial state.[27−29]

If the free energy surfaces of initial and final states, i.e. when the electron is localized at the donor or acceptor, respectively, are parabolic as is generally assumed and intramolecular structural rearrangements as well as solvent reorganization comprise only classical modes, $\rho(E_f)$ is a Gaussian function of the free energy of reaction $\Delta G°$, with variance $\sigma^2 = 2\lambda k_B T$,

$$\rho(E_f) = \frac{1}{[4\pi\lambda k_B T]^{1/2}} \exp\left\{-\frac{(1 + \Delta G°)^2}{4\lambda k_B T}\right\} \tag{9}$$

where $\lambda = \lambda_v + \lambda_S$ is the total reorganization energy containing intramolecular (λ_v, innersphere) and outersphere (λ_S, solvent) contributions, and k_B and T are Boltzmann's constant and temperature, respectively.

The free energy of activation $\Delta G^‡$ of electron transfer, included in the density of final states $\rho(E_f)$, is given by the Marcus equation[30]

$$\Delta G^‡ = (\lambda + \Delta G°)^2/4\lambda \tag{10}$$

which provides a parabolic free energy relationship for $\Delta G^‡$. The center of the Gaussian, i.e. activationless electron transfer, is realized for $-\Delta G° = \lambda$. Separated by this condition are the two regimes of the function $\Delta G^‡$ ($\Delta G°$), where $-\Delta G° < \lambda$ (normal region) and $-\Delta G° > \lambda$ (Marcus-inverted region), respectively (Figure 9).

In the normal region, the electron transfer rate is enhanced by a decrease of the free energy of reaction as predicted by traditional free energy relationships[31] and the Hammond postulate,[32] while in the inverted regime the electron transfer rate decreases with increasing driving force $-\Delta G°$. This result, which is rather unexpected within the framework of traditional chemical reaction rate theory, is however quite common in the theory of radiationless molecular electronic processes, where it

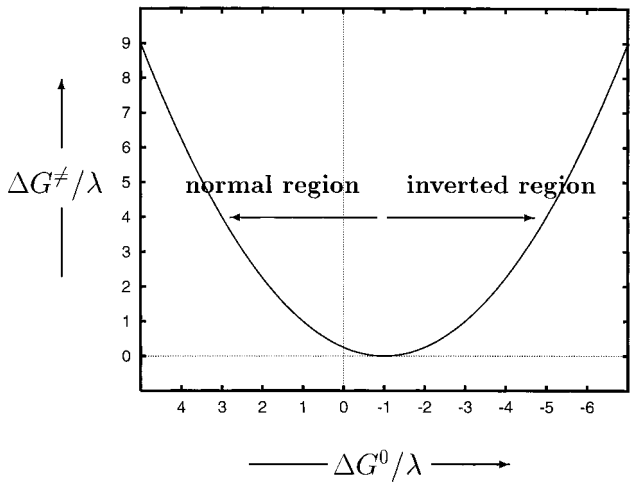

Figure 9. Free energy of activation $\Delta G^‡$of an electron transfer reaction as a function of the reaction free energy $\Delta G°$ according to classical Marcus theory. $\Delta G^‡$ and $\Delta G°$ are given in units of the reorganization energy λ.

is known under the name energy gap law (see ref 27 and references cited therein).

For interpretating the pH dependence of the luminescence quantum efficiency of fluorescent PeT sensors like **F221** and **F222**, the free energy of photoinduced electron transfer may be considered a control parameter, which can be influenced by the binding of protons to the nitrogen atoms of the cryptand, i.e. the electron donor. Since such a protonation of the donor most probably leads to an endergonic shift of the eT free energy, a reduction of the quenching rate is to be expected, when we assume that the systems under study are located in the normal region and that the energy of reorganization is not altered significantly upon protonation. However, even if the latter argument did not hold, a reduction of the number of thermally excitable modes due to an increased rigidity of the molecular framework in the protonated state would most probably lead to a decrease of the eT rate in the normal region.

(b) Free Energy of Photoinduced Electron Transfer: The Weller Equation. The free energy of a photoinduced electron transfer reaction can be calculated if the respective redox potentials of donor and acceptor as well as the energy of the vibronic 0−0 transition of the locally excited (LE) donor or acceptor are known. The resulting relation

$$\Delta G^\circ_e = \Delta G^\circ_g - \Delta E^{(00)} + C + S = G^\circ(A/A^-) - G^\circ(D^+/D) - \Delta E^{(00)} + C + S \quad (11)$$

is known as the Weller equation,[33] where ΔG°_e denotes the free energy of eT in the excited state and $\Delta G^\circ_g = G^\circ(A/A^-) - G^\circ(D^+/D)$ is the free energy of eT in the electronic ground state. The extra internal energy $\Delta E^{(00)}$ of the electronically excited donor or acceptor provides an additional negative contribution to the PeT reaction free energy ΔG°. C denotes a Coulombic term taking into account the electrostatic attraction or repulsion of reactants and products, respectively. For the present charge separation, C is negative and is expected to significantly stabilize the intramolecular radical ion pair produced. Solvation terms S are required when redox potentials have to be corrected for different solvent environments. When eq 11 is used to predict excited state eT energetics, care must be taken that the following conditions are met, at least approximately:

(i) Electronic excitation of electron donor or acceptor does not lead to a significant change in entropy of the internally equilibrated excited state with respect to the ground state. For locally excited states (LEs) of rigid aromatics this is generally a good approximation.

(ii) Electronic overlap of donor and acceptor within the PeT precursor complex has to be weak; i.e. PeT should proceed nonadiabatically or be at least weakly adiabatic, in order for the redox potentials of isolated redox components to hold also at the finite distances of approach realized in the reaction complex. Thus, if donor and acceptor do not mutually perturb their respective electronic structures and the change of electric monopoles provides by far the leading contribution of intermolecular interaction to the PeT reaction free energy, the Weller equation can be employed in the form given above. We note here that charge transfer absorption bands could not be observed for **F221** and **F222** when comparing the optical absorption spectra of these coumarino cryptands with that of **I**. Therefore, the weak-coupling assumption seems to be applicable for our donor−acceptor systems.

(c) Application to pH-Dependent Fluorescence Quenching of the Mono- and Deprotonated F221. In the following, relatively simple estimates of the PeT thermodynamic driving forces for the fully deprotonated **F221** and **F221**H^+ will be given. They are based on cyclic voltammetry data for the isolated **[2.2.1]** cryptand and the coumarin chromophore **I** (cf. Table 6). Due to the observed instability of the respective radical ions produced by oxidation and reduction, respectively, CV measurements for the coumarino cryptands **F221** and **F222** were not undertaken.

With redox potentials in methylene chloride and electronic excitation energy in water given by $E^\circ(D^+/D) = +1.13$ V, $E^\circ(A/A^-) = -1.56$ V and $\Delta E^{(00)} = 3.060$ eV, respectively, the free energy ΔG° of photoinduced electron transfer is

$$\Delta G^\circ = +1.56 \text{ eV} - (-1.13 \text{ eV}) - 3.060 \text{ eV} + C + S = -0.37 \text{ eV} + C + S \quad (12)$$

Without solvational and Coulombic corrections, photoinduced charge separation for the deprotonated **F221** in methylene chloride is therefore slightly exergonic.

(1) Solvation Term S. Assuming that the solvation correction is only due to the difference in ionic solvation of the radical ions in CH_2Cl_2 and water (no specific solvation effects), S can be calculated from the Born equation (see ref 34)

$$E_{solv} = -\frac{(Ze_0)^2}{4\pi\epsilon_0}\frac{1}{2r_{D(A)}}\left\{1 - \frac{1}{\epsilon_S}\right\} \quad (13)$$

where r_D and r_A are the radii of (oxidized) donor and (reduced) acceptor, respectively, ϵ_S is the static dielectric constant of the respective solvent, and Ze_0 is the charge of the respective radical ion. S is then a sum of two terms,

$$S = S_+ + S_- = \{E^+_{solv}(\epsilon_S^{new}) - E^+_{solv}(\epsilon_S^{old})\} + \{E^-_{solv}(\epsilon_S^{new}) - E^-_{solv}(\epsilon_S^{old})\} \quad (14)$$

where $\epsilon_S^{old} = 9.1$ (dichloromethane) and $\epsilon_S^{new} \cong 80$ (water). Estimating the reactant radii to be between $r_D = 2.5$ and 3.0 Å and $r_A = 3.0$ and 3.5 Å, as obtained from conformational analyses by Lanig[8,11] and our own simulations,[35] S_+ and S_- values vary between $S_+ = -0.281$ and -0.234 eV as well as $S_- = -0.234$ and -0.200 eV, respectively, leading to S values between -0.515 and -0.434 eV. With S terms included, the PeT reaction is now already markedly exergonic for the deprotonated **F221** in water.

(2) Coulombic Term C. The C terms can be obtained from the model of Suppan[34] for contact ion pairs formed by spherical ions. The respective equation is

$$C = -\frac{(Ze_0)^2}{4\pi\epsilon_0}\left\{\frac{a}{R^2 n_M{}^2} + \frac{1}{R\epsilon_S}\left(1 - \frac{a}{R}\right)\right\} \quad (15)$$

where $a = (r_D + r_A)/2$ denotes the mean value of donor and acceptor radii, R is the center-to-center distance of spheres, and ϵ_S is the static dielectric constant of the solvent (water) as above. n_M is an estimate for the molecular refractive index, where $n_M{}^2$ is a measure of the electronic polarizability of eT precursor and successor complexes. Since reaction products carry opposite charges, C is negative.

With again r_D between 2.5 and 3.0 Å, r_A between 3.0 and 3.5 Å, and R between 6.0 and 6.5 Å, $n_M{}^2 \cong 2$ and $\epsilon_S \cong 80$, Coulombic contributions between $C = -0.566$ eV and $C = -0.568$ eV are obtained. Electrostatic stabilization of the radical ion pair produced through charge separation therefore comprises another important part of the PeT reaction free energy. Tables 7 and 8 summarize the different contributions to the PeT

TABLE 7: Contributions to the Free Energy $\Delta G°_e$ of PeT (in the Excited State) for the Deprotonated State of F221 in Water; $T = 25$ °C

$G°(A/A^-) - G°(D^+/D)$[a]		+2.69 eV
$-\Delta E^{(00)}$ [b]		−3.06 eV
	$r_D = 2.5$ Å, $r_A = 3.0$ Å, $R = 6.0$ Å	$r_D = 3.0$ Å, $r_A = 3.5$ Å, $R = 6.5$ Å
S[c] (eV)	−0.515	−0.434
C[d] (eV)	−0.566	−0.568
$\Delta G°_e$ (eV)	−1.451	−1.372

[a] Calculated from redox potential of donor and acceptor in CH_2Cl_2 (cf. Table 6). [b] Obtained as the arithmetic mean of the experimental absorption and fluorescence maxima of deprotonated **F221** in water. [c] Theoretical correction of the solvation energies (cf. eqs 11−14) when PeT reactants and products are transferred from CH_2Cl_2 to water. [d] Theoretical electrostatic stabilization in water of the intramolecular radical ion pair produced via photoinduced charge separation (cf. eqs 11, 12, 15).

TABLE 8: Contributions to the Free Energy $\Delta G°_e$ of PeT for F221H$^+$ in Water; $T = 25$ °C

$G°(A/A^-) - G°(D^+/D)$[a]		+2.69 eV
$-\Delta E^{(00)}$ [b]		−3.06 eV
	$r_D = r_{NH^+} = 2.5$ Å, $r_A = 3.0$ Å, $R = 6.0$ Å, $R_{NN} = 5.5$ Å [e]	$r_D = r_{NH^+} = 3.0$ Å, $r_A = 3.5$ Å, $R = 6.5$ Å, $R_{NN} = 6.0$ Å [e]
S[c] (eV)	−0.515	−0.434
C[d] (eV)	−0.520	−0.520
$\Delta G°_e$ (eV)	−1.405	−1.324

[a] Calculated from redox potential of donor and acceptor in CH_2Cl_2 (cf. Table 6). [b] Obtained as the arithmetic mean of the experimental absorption and fluorescence maxima of **F221**H$^+$ in water. [c] Theoretical correction of the solvation energies (cf. eqs 11−14) when PeT reactants and products are transferred from CH_2Cl_2 to water. [d] Theoretical electrostatic stabilization in water of the intramolecular radical ion pair produced via photoinduced charge separation (cf. eqs 11, 12, 15). [e] With respect to the interaction with the reduced acceptor, the NH^+ group was treated like the oxidized donor, i.e. $R_{NH^+A^-} = R$.

energetics as well as the total free energy $\Delta G°$ for the fully deprotonated **F221** (Table 7) and **F221**H$^+$ (Table 8) in water.

In the case of **F221**H$^+$, where the dominant effect is related to the protonation of one nitrogen atom, two additional C terms are to be expected in the Weller equation, due to destabilization of the oxidized donor and stabilization of the reduced acceptor, respectively. Additional S terms have been neglected, since the charge of the protonated N-atom should not vary significantly during PeT. The effective radius of the protonated N-atom was set to $r_{NH^+} = 2.5$ or 3.0 Å. The corresponding N−N distances were $R_{NN} = 5.5$ and 6.0 Å, respectively. With regard to interactions between the NH^+ group and reduced acceptor, NH^+ was treated as the oxidized donor. Obviously, stabilizing and destabilizing effects induced by monoprotonation nearly cancel each other. The shorter distance between the protonated nitrogen and the electron donor N-atom, however, leads to a net destabilization of PeT products and a weak endergonic shift of energetics for **F221**H$^+$ of approximately 1.075−1.091 kcal/mol as compared to the deprotonated **F221**.

Discussion

The experimental results obtained with **F221** and **F222** as well as with three model compounds indicate that the diprotonated state FH_2^{2+} of the fluorescent cryptands and of the model compound **IIb** exhibit a comparatively high quantum yield around 0.6 and are characterized by a single lifetime around 5.4 ns, similar to model compounds **I** and **IIa.** Full protonation of **F221** and **F222** apparently leads to a comparatively unflexible conformation of the cryptand moiety where one or both protons could be located inside the cavity, which, due to the larger cavity, seems to be more probable for **F222** than for **F221**. In a modeling study, Wipff et al.[23] have suggested such a structure for the protonated form of **[2.2.2]**. The unexpected low pK_{a1} value found for **F222** could in contrast to the values obtained for **F221** and **IIb** also be consistent with such a structural conclusion. Deprotonation of FH_2^{2+} of **F221**, **F222**, and **IIb**, leading to the state FH^+, is accompanied by about a 10-fold reduction of the quantum yield for **F221**, 40-fold for **F222**, and 20-fold for **IIb**. The lifetime of the monoprotonated state is around 1.0 ns for **F221** and 0.19 ns for **F222**. Upon complete deprotonation, a further but small reduction of the quantum yield is found. Because values of the lifetimes above pH 7.5 appear to have a tendency to decrease (cf. Table 5), we can assume that F has a slightly smaller lifetime than that of FH^+.

Relating the experimental results obtained from steady-state and time-resolved fluorescence spectroscopy for **F221** and **F222** in aqueous solution at different pH values to our theoretical considerations based upon electron transfer theory and to cyclic voltammetry redox potential data allows a rationalization of the observed pH dependence of fluorescence quenching in terms of PeT. The central parameter responsible for the variation of the rate of fluorescence quenching, which is determined by the degree of protonation of **F221** and **F222**, seems to be the free energy of PeT.

By means of simple estimations based on the Weller equation using redox potential data obtained from cyclic voltammetry for the parent cryptand [**2.2.1**] in its deprotonated state and the chromophore **I** in CH_2Cl_2, it is shown that PeT is thermodynamically favored for both the mono- and deprotonated forms of **F221** in aqueous solution, where solvation and Coulombic stabilization of the radical ion pair produced via charge separation contribute significantly to the excited state reaction energetics. After applying the solvation correction for the transformation from CH_2Cl_2 to water, our CV data seem to be reasonably close to the values obtained by Ritzler et al.[36] for the one-electron oxidation of **[2.2.1]** and **[2.2.2]** in water. Most importantly, the endergonic shift of the PeT reaction free energy of 1.1 kcal/mol (0.05 eV) upon monoprotonation predicted by our simple electrostatic considerations are equal to about half of the endergonic shift of the **[2.2.2]** oxidation potential upon protonation observed by Ritzler et al. This may be attributed to the electrostatic stabilization of the photoreduced chromophore by the proton in our systems.

While the obtained small endergonic shift of PeT free energy upon monoprotonation may not lead to distinguishable fluorescence lifetimes for the mono- and deprotonated states of **F221** and also for the same states of **F222** (note, however, the small but clearly detectable decrease in fluorescence intensity upon formation of deprotonated **F221** at high pH (Figure 5)), it is expected that fluorescence quenching is completely blocked in the diprotonated form. Ritzler et al, report a lower bound of approximately 1 eV for the endergonic shift of the one-electron oxidation of **[2.2.2]**H_2^{2+} with respect to **[2.2.2]**H^+. This is in accord with the experimental findings that by varying the pH, the fluorescent ensemble is shifted from a highly luminescent state (FH_2^{2+}) with longer lifetime at low pH to a weakly fluorescent subensemble (FH^+ and F) with shorter lifetime.

By using FH_2^{2+} as a reference state and assuming that it is unaffected by photoinduced eT, the rate coefficient k^{PeT} of quenching by electron transfer in the case of FH^+ and F can be obtained as

$$k^{PeT} = \frac{1}{\tau_{FH^+,F}} - \frac{1}{\tau_{FH_2^{2+}}} = \frac{1}{\tau_2} - \frac{1}{\tau_1} \qquad (16)$$

where $\tau_{FH_2^{2+}}$ is identified as the fluorescence lifetime τ_1 dominating at low pH and τ_{FH^+} is set equal to the second lifetime τ_2 appearing in the time-resolved fluorescence decay at higher pH values. Using the fixed lifetimes $\tau_1 = 5.4$ ns and $\tau_2 = 0.19$ ns for all pH values (Table 5), an electron transfer rate coefficient of $k^{PeT} = 5.08$ ns^{-1} for the states FH^+ and F is obtained. Such an order of magnitude is reasonable for a possibly activated, nonadiabatic excited state electron transfer process.[37]

Since the coupling between electron donor (N-atoms) and electron acceptor (excited coumarin chromophore) via the saturated ethylene oxide bridges of our cryptands can be regarded as weak, the postulated PeT reaction is expected to be controlled by the electronic donor−acceptor interaction. As a consequence of alkali ion complexation, electronic levels of low energy are introduced into the system which may open new pathways for electron tunneling and may consequently lead to an increase of the effective electronic coupling between donor and acceptor. Therefore, cryptates such as **Na^+⊂F221** and **K^+⊂F222**, which exhibit a more complex fluorescence behavior, will be addressed in a subsequent publication.

Acknowledgment. The financial support of PROCOPE, the German Academic Exchange Organization (D.A.A.D) and the Max-Planck Society to P.B. is acknowledged. G.K. is grateful for financial support by the Fonds der Chemischen Industrie, the Deutsche Forschungsgemeinschaft, the Max-Planck Society during his stay in Frankfurt/Main and the German−French exchange program PROCOPE. We wish to thank Dr. A.-M. Albrecht-Gary, Prof. J.-M. Lehn, and Prof. G. Wipff of the University of Strasbourg for helpful and stimulating discussions. We appreciate the help of Prof. M. Schmittel and his co-workers, Dr. A. Burghart and H. Ammon, in providing us the opportunity to obtain cyclovoltammetric information on our compounds.

References and Notes

(1) Lehn, J.-M. *Supramolecular Chemistry*; VCH: Weinheim, Germany, 1995.
(2) Bissell, R. A.; de Silva, A. P.; Gunaratne, H. Q. N.; Lynch, P. L. M.; Maguire, G. E. M.; McCoy, C. P.; Sandanayake, K. R. A. S. *Top. Curr. Chem.* **1993**, *168*, 223.
(3) Smith, G. A.; Hesketh, T. R.; Metcalfe, J. C. *Biochem. J.* **1988**, 227.
(4) Fages, F.; Desvergne, J.-P.; Kampke, K.; Bouas-Laurent, H.; Lehn, J.-M.; Meyer, M.; Albrecht-Gary, A.-M. *J. Am. Chem. Soc.* **1993**, *115*, 3658.
(5) Golchini, K.; Mackovic-Basic, M.; Gharib, S. A.; Masilamani, D.; Lucas, M. E.; Kurtz, I. *Am. J. Physiol.* **1990**, *258*, F438.
(6) Crossley, R.; Goolamali, Z.; Sammes, P. G. *J. Chem. Soc., Perkin Trans. 2* **1994**, 1615.
(7) Kastenholz, F. Ph.D. Thesis, Max-Planck-Institute of Biophysics, Frankfurt, and University of Köln, 1993. Separate publication of synthesis and crystal structure in preparation.
(8) Kastenholz, F.; Grell, E.; Bats, J. W.; Quinkert, G.; Brand, K.; Lanig, H.; Schneider, F. W. *J. Fluoresc.* **1994**, *4*, 243.
(9) Warmuth, R.; Gersch, B.; Kastenholz, F.; Lehn, J.-M.; Bamberg, E.; Grell, E. In *The Sodium Pump*; Bamberg, E., Schoner, W., Eds.; Steinkopff: Darmstadt, Germany, 1994; p 621.
(10) Dietrich, B.; Dillworth, B.; Lehn, J.-M.; Souchez, J.-P.; Cesario, M.; Guilhelm, J.; Pascard, C. *Helv. Chim. Acta* **1996**, *79*, 569.
(11) Lanig, H. Ph.D. Thesis, University of Würzburg, 1994.
(12) Bayer, V.; Pastor, R.; Cambon, A. *J. Fluor. Chem.* **1982**, *20*, 187.
(13) Bayzer, A. *Experentia* **1964**, *20*, 233.
(14) Lakowicz, J. R. *Principles of Fluorescence Spectroscopy*; Plenum Press: New York, 1986; p 41.
(15) Bridges, J. W. In *Standards in Fluorescence Spectrometry Ultraviolet Spectrometry Group*; Miller, J. N., Eds.; Chapman and Hall: London, 1981; p 68.
(16) Guilbault, G. G. *Practical Fluorescence;* Dekker: New York, 1973; p 11.
(17) Marquardt, D. W. *J. Soc. Ind. Appl. Math.* **1963**, *11*, 431.
(18) Hof, M.; Schleicher, J.; Schneider, F. W. *Ber. Bunsen-Ges. Phys. Chem.* **1989**, *93*, 1377.
(19) Arnek, R.; Sillen, L. G.; Wahlberg O. *Arkiv. Kemi* **1968**, *31*, 353.
(20) Brauner, P.; Sillen, L. G.; Whiteker, R. *Arkiv. Kemi* **1968**, *31*, 365.
(21) Sillen, L. G.; Warnqvist, B. *Arkiv. Kemi* **1968**, *31*, 377.
(22) Lehn, J. M.; Sauvage, J. P. *J. Am. Chem. Soc.* **1975**, *97*, 6700.
(23) Auffinger, P.; Wipff, G. *J. Incl. Phenom. Mol. Recognit. Chem.* **1991**, *11*, 71.
(24) Brand, K. Ph.D. Thesis, University of Würzburg, 1993.
(25) Cox, B. G.; Knop, D.; Schneider, H. *J. Am. Chem. Soc.* **1978**, *100*, 6002.
(26) Bissell, R. A.; de Silva, A. P.; Gunaratne, H. Q. N.; Lynch, P. L. M.; Maguire, G. E. M.; McCoy, C. P.; Sandanayakae, K. R. A. S. *Top. Curr. Chem.* **1993**, *168*, 223.
(27) Klessinger, M.; Michl, J. *Lichtabsorption und Photochemie Organischer Moleküle*; VCH: Weinheim, Germany, 1989.
(28) Kestner, N. R.; Logan, J.; Jortner, J. *J. Phys. Chem.* **1974**, *78*, 2148.
(29) Kuznetsov, A. M. *Charge Transfer Processes in Physics, Chemistry and Biology;* Gordon and Breach: Luxembourg, 1995.
(30) Marcus, R. A. *Angew. Chem.* **1993**, *105*, 1161.
(31) Lowry, T. H.; Schueller-Richardson, K. *Mechanism and Theory in Organic Chemistry*; Harper & Row: New York, 1987.
(32) Hammond, G. S. *J. Am. Chem. Soc.* **1955**, *77*, 334.
(33) Rehm, D.; Weller, A. *Isr. J. Chem.* **1970**, *8*, 259.
(34) Suppan, P. *Chimia* **1988**, *10*, 31.
(35) Käb, G. Ph.D. Thesis, University of Würzburg, 1998.
(36) Ritzler, G.; Peter, F.; Gross, M. *J. Electroanal. Chem.* **1983**, *146*, 285.
(37) Bolton, J. R., Mataga, N., McLendon, G., Eds. *Electron Transfer in Inorganic, Organic and Biological Systems;* American Chemical Society: Washington, D.C., 1991.